INTERFACE

royalsocietypublishing.org/journal/rsif

Research

Cite this article: Htut KZ et al. 2021 Correlation between protein secondary structure and mechanical performance for the ultra-tough dragline silk of Darwin's bark spider. J. R. Soc. Interface 18: 20210320. https://doi.org/10.1098/rsif.2021.0320

Received: 17 April 2021
Accepted: 24 May 2021

Subject Category:
Life Sciences–Engineering interface

Subject Areas:
biomaterials, biomimetics, biophysics

Keywords:
spider silk, protein secondary structure, mechanical properties, Raman spectroscopy

Authors for correspondence:
Todd A. Blackledge
e-mail: tab27@uakron.edu
Ali Dhinojwala
e-mail: ali4@uakron.edu

†These authors contributed equally to this study.

Electronic supplementary material is available online at https://doi.org/10.6084/m9.figshare.c.5448661.

THE ROYAL SOCIETY PUBLISHING

Correlation between protein secondary structure and mechanical performance for the ultra-tough dragline silk of Darwin's bark spider

K Zin Htut[1,†], Angela M. Alicea-Serrano[2,†], Saranshu Singla[1], Ingi Agnarsson[3], Jessica E. Garb[4], Matjaž Kuntner[5,6], Matjaž Gregorič[5], Robert A. Haney[7], Mohammad Marhabaie[8], Todd A. Blackledge[2] and Ali Dhinojwala[1]

[1]School of Polymer Science and Polymer Engineering, and [2]Department of Biology, Integrated Bioscience Program, The University of Akron, Akron, OH 44325, USA
[3]Department of Biology, University of Vermont, Burlington, VT 05405, USA
[4]Department of Biological Sciences, University of Massachusetts Lowell, Lowell, MA 01854, USA
[5]Jovan Hadži Institute of Biology ZRC SAZU, Novi trg 2, 1000 Ljubljana, Slovenia
[6]Department of Organisms and Ecosystems Research, National Institute of Biology, Večna pot 111, 1000 Ljubljana, Slovenia
[7]Department of Biology, Ball State University, Muncie, IN 47306, USA
[8]The Steve and Cindy Rasmussen Institute for Genomic Medicine, Nationwide Children's Hospital, Columbus, OH 43215, USA

KZH, 0000-0002-3876-2663; AMA-S, 0000-0002-6255-7838; SS, 0000-0002-0690-3740; IA, 0000-0003-4548-7927; JEG, 0000-0001-7428-8156; MK, 0000-0002-0057-2178; MG, 0000-0002-4882-4282; RAH, 0000-0002-3742-3395; MM, 0000-0002-5609-2915; TAB, 0000-0002-8166-5981; AD, 0000-0002-3935-7467

The spider major ampullate (MA) silk exhibits high tensile strength and extensibility and is typically a blend of MaSp1 and MaSp2 proteins with the latter comprising glycine–proline–glycine–glycine-X repeating motifs that promote extensibility and supercontraction. The MA silk from Darwin's bark spider (*Caerostris darwini*) is estimated to be two to three times tougher than the MA silk from other spider species. Previous research suggests that a unique MaSp4 protein incorporates proline into a novel glycine–proline–glycine–proline motif and may explain *C. darwini* MA silk's extraordinary toughness. However, no direct correlation has been made between the silk's molecular structure and its mechanical properties for *C. darwini*. Here, we correlate the relative protein secondary structure composition of MA silk from *C. darwini* and four other spider species with mechanical properties before and after supercontraction to understand the effect of the additional MaSp4 protein. Our results demonstrate that *C. darwini* MA silk possesses a unique protein composition with a lower ratio of helices (31%) and β-sheets (20%) than other species. Before supercontraction, toughness, modulus and tensile strength correlate with percentages of β-sheets, unordered or random coiled regions and β-turns. However, after supercontraction, only modulus and strain at break correlate with percentages of β-sheets and β-turns. Our study highlights that additional information including crystal size and crystal and chain orientation is necessary to build a complete structure–property correlation model.

1. Introduction

The dragline or major ampullate (MA) silk produced by orb-weaving spiders is used as a lifeline and as supporting radii for the capture silk in webs and possesses excellent tensile strength, elasticity and the ability to absorb energy before reaching breaking point. The high toughness allows MA silk to absorb the tremendous kinetic energy of flying insects when they hit the web [1–3]. Generally, spider MA silk outperforms high-energy absorbing synthetic polymers such as Kevlar by

approximately 300% on a volume-to-volume comparison [1,4]. In 2010, a new species, Darwin's bark spider (*Caerostris darwini*), was described [5], which builds the largest known orb webs across ponds and rivers in Madagascar (web area up to 2.8 m^2 and bridgelines up to 25 m) [6,7]. To our knowledge, the toughness of the dragline silk of *C. darwini* (350 ± 93 MPa) surpasses by two to three times any other previously investigated dragline silk (10–230 MPa). Understanding the molecular origin of the exceptionally high toughness of *C. darwini* dragline silk is essential not only for elucidating the evolutionary root of its foraging strategy but also for designing biomaterials with exceptional mechanical properties.

The dragline silk of *C. darwini* incorporates a novel MaSp4 (major ampullate spidroin 4) [8] with MaSp1 (major ampullate spidroin 1) and MaSp2 (major ampullate spidroin 2), which are typically found in the dragline silk from other orb-weaving spider species [9–11]. cDNA analyses of MA glands of orb-weaving spiders reveal that MaSp1 contains glycine (G)-rich tripeptide sequences such as GGX and GXG (where X = glutamine (Q), tyrosine (Y), leucine (L) or arginine (R)), and consecutive [4–7] polyalanine (A) motifs [12–14]. On the other hand, MaSp2 contains proline (P)-rich pentapeptide sequences such as GPGQQ and GPGGX (where X = A, serine (S) or Y) [11,15,16]. Some of the proline gets converted to hydroxy proline during the post-translational modification process [17,18]. Researchers have shown a positive correlation between the amount of hydroxy proline and stretchability of silk fibres, in particular flagelliform silk [17–19]. MaSp4 contains a high percentage of proline based on the predicted amino acid sequence, although the overall proline levels in *C. darwini* silk and silk dope are not unusual (dragline silk (6.4–7.3%; $n = 3$) and MA silk dope (11.7%; $n = 1$)) [8]. However, the neighbouring position of proline with respect to glycine (GPGPQ) in MaSp4 of *C. darwini* is different from that of MaSp2 of known species. In addition, MaSp4 has a high abundance of these GPGPQ motifs (44–52% of the repetitive region) and lacks the consecutive polyalanine domains found in MaSp1.

The primary amino acid sequence dictates the secondary structure of proteins, which is expected to influence the mechanical properties. Meta-analysis using phylogenetic comparative tests performed on various species also showed that spidroin expression is found to be integral to the mechanical properties of the MA silk [20]. For example, alanine and glycine promote strength-inducing β-sheet formation in MaSp1 by stacking together to form nanocrystals, while the bulky hydroxy proline group disrupts β-sheet formation and instead promotes β-turns since the –OH group in the hydroxy proline stabilizes the amorphous region with H-bonding in the β-spirals [19,21–23]. The combined percentage of glycine and proline has been shown to influence the silk elastin-like behaviour of MA silk, thereby highlighting the importance of proline in silk elasticity [24,25]. Thus, Garb *et al*. [8] hypothesized that the high proline content in MaSp4 could promote stretchiness of *C. darwini* MA silk by forming β-spirals owing to differences in the amino acid arrangement (GPGPQ in MaSp4 versus GPGQQ and GPGGX in MaSp2).

Differences in the expression of MaSp proteins lead to variations in the mechanical properties of dragline silk [11,19,26,27]. Also, spiders can potentially vary the expression of different MaSp proteins in the MA silk to tune web performance both physiologically [28,29] and evolutionarily [30]. *C. darwini* is also hypothesized to incorporate the MaSp4 protein to tune MA silk chemical composition and performance [8]. However, while these studies show the correlations between the chemical composition and performance of MA silk, they do not address how chemical composition results in specific molecular structures determining variation in the performance of MA silk. Hence, we still do not know the influence of MaSps on the variation in the secondary structure of proteins and the mechanical properties of the *C. darwini* MA silk. *C. darwini* has a longer MA duct than other spider species, which might aid in achieving tougher silk (i) by interacting with MaSp4 in the duct or (ii) on its own by increasing the retention time of the dope in the lumen of the duct. The increased retention time could affect the water uptake [31–35], ion exchange [36,37], pH gradient [36,38], shear force [39–41] and ultimately the viscosity along the duct as well as when it reaches the end of the duct [39,42]. Molecular models for viscosity and mechanical properties reveal a liquid-crystalline-like behaviour of the dope in high concentration in which stiffness-inducing β-sheet crystals are formed [37,42].

Generally, besides the protein composition in the spinning dope, a number of spinning conditions such as humidity [43], temperature [39,43] and spinning velocity [39,40,44,45] could affect the material properties of spider silk. In one study, the silk mechanical properties such as resilience, ductility and thread diameters were observed to be different depending on whether the silk was drawn using low or high drawing speeds and temperature [39]. However, other studies have found robustness in these properties reeled at different speeds and humidity [46]. Supercontraction helps to understand how molecular information dictated by MaSp composition influences material performance by removing many of the effects of silk spinning, especially reeling speed and shear forces, which can alter the molecular structure and hence performance. During supercontraction, MA silk swells laterally and shrinks longitudinally by up to 50% of its length after exposure to high humidity [40,47]. The contraction of silk is a consequence of water molecules disrupting the intermolecular hydrogen bonds in the amorphous regions, leading to an increase in molecular chain mobility to a more disorganized, higher entropy state [48–50].

The structure–function relationship between the protein secondary structure and mechanical properties has been elucidated for various spider silks, such as *Nephila clavipes* (now named *Trichonephila clavipes*) [15,51], *Nephila edulis* (now named *Trichonephila edulis*) [16,52,53], *Nephila pilipes* [54] and silkworm silks such as *Antheraea pernyi* [55]. However, a similar structure–property relationship has not been investigated for *C. darwini* MA silk. In the present work, we aim to investigate the hypothesized influence of MaSp4 on the composition of relative protein secondary structures and correlate them with the mechanical properties of dragline silk of *C. darwini*. Previously, ^{13}C dipolar decoupling–magic angle spinning nuclear magnetic resonance (DD-MAS NMR) was used to demonstrate the dependence of protein secondary structures (the percentage of unordered regions, β-sheets, helices and β-turns) on the primary amino acid sequences of silk proteins [56–58]. Also, dynamic nuclear polarization (DNP) NMR was used to enhance the NMR signal to elucidate the dependency of silk primary amino acid sequences on the expression of MaSp [19]. In another study, the percentage of various protein secondary structures was extracted using Raman spectroscopy for the MA and flagelliform silk of *T. clavipes* [15,59–64]. The higher tensile strength of MA silk relative to flagelliform silk was rationalized on the basis of higher β-sheet content of the MA silk, highlighting the importance of β-sheets in tensile

strength [15]. Thus, understanding the protein secondary structure composition for *C. darwini* could aid in explaining its exceptional mechanical properties.

Here, we use Raman spectroscopy and tensile testing to correlate relative protein secondary structure composition with the mechanical properties of *C. darwini* MA silk obtained from the field in Madagascar. To better understand how the presence of proline-rich MaSp4 in *C. darwini* MA silk may influence protein secondary structure composition, we also compare the variation in relative protein secondary structure composition and material properties across four other spider species with varying proline content. We further compare the mechanical properties of these silks after exposure to high humidity (greater than 70% RH), which allows them to undergo supercontraction and remove some of the effects of spinning conditions on silk properties [47,50,65,66]. We test two hypotheses regarding the properties of composite MA fibres: first, the addition of proline-rich MaSp4 to a mix of MaSp1 and MaSp2 in *C. darwini* MA silk results in a higher percentage of β-turns than in silks from other spider species; second, the high β-turn content in *C. darwini* MA silk results in higher extensibility, thereby explaining its high toughness.

2. Methods

2.1. Spider care and silk collection

Five spider species were chosen based on the variation in the proline content of their MA silk: *Argiope trifasciata* (Pro ~11%) [11], *Larinioides cornutus* (Pro ~12%), *C. darwini* (Pro ~7%) [8], *Parasteatoda tepidariorum* (Pro ~7%) and *T. clavipes* (Pro ~3%) [20] (electronic supplementary material, table S2). A detailed description of the method used for amino acid composition analysis can be found in the electronic supplementary material. Generally, the percentage of proline in the MA silk is used as an indicator of the ratio of MaSp1 to MaSp2, because MaSp1 is almost proline free and MaSp2 is abundant in proline [11,12,25,28,67–69]. The proline-rich MaSp4 is newly described from *C. darwini* [8] and has not previously been detected in the MA silk of the other species examined in this study. However, there is always a possibility of the discovery of new MaSps in the future. *A. trifasciata* and *L. cornutus* were collected from the University of Akron field station at the Bath Nature Preserve (Bath, OH), while *P. tepidariorum* were collected from the University of Akron campus as well as homes in the greater Akron, OH region. *T. clavipes* spiders were purchased from BugsofAmerica.com. The spiders were kept inside cages (40 × 40 × 10 cm) at the University of Akron and fed weekly with house crickets (*Acheta domesticus*). We started reeling the MA silk two weeks after the spiders were collected to normalize their food source. The reeling procedure involved first anaesthetizing spiders with CO_2 for 30–50 s and then securing the spiders on a glass platform using a pressure-sensitive adhesive tape. After allowing the spiders to recover for about 5 min, the MA silk was forcibly reeled at a speed of 2 mm s^{-1} only from the MA glands (verified under a stereomicroscope) at ambient temperature and humidity (55–64% RH). The MA silk of *C. darwini* was collected directly in the field from their MA glands, the same day as the spiders were collected, using a portable electromotor at a speed of 6.5 cm s^{-1}.

2.2. Raman spectroscopy

2.2.1. Measurement procedure

Raman spectra were recorded at 22 ± 0.5°C and approximately 30% RH using a LabRam HR Micro Raman Spectrometer (Horiba) coupled to an Olympus BX41 motorized stage microscope using a 532 nm line of an Nd:YAG laser beam. To perform Raman measurements, filaments of MA silk (approximately 2–5 µm in diameter) were mounted on pieces of 12.58-mm-wide paper cardboard with double-sided tape (electronic supplementary material, figure S1). A 100× objective (0.9 NA; Olympus) was used to focus the beam on the sample. The intensity of the laser beam at the sample was kept low (1.5 mW) to avoid sample damage. The hole and entrance slit of the monochromator were fixed at 400 and 100 µm, respectively, and the exposure time was set to 60 s. Ten scans were accumulated over a period of 20 min for each sample to achieve the best signal-to-noise ratio. Spectra were collected using a 2.5 cm open Peltier-cooled charge-coupled device detector (1024 × 256 pixels) with a 1200 lines mm^{-1} holographic grating.

2.2.2. Curve fitting

No smoothing was done prior to the fitting. Spectra were fitted with the Gaussian function using the multi-peak fitting package available in IGOR pro (WaveMetrics Inc., Portland, OR, USA). The relative protein secondary structures were calculated using a well-known procedure available in the literature [15,59,61–63,70,71], in which the amide I region (1600–1700 cm^{-1}) is decomposed into various peaks corresponding to different secondary structures. The number of peaks and their location used to fit the amide I region were determined by calculating the second derivative of the observed spectra. In all spectra, five bands corresponding to the protein secondary structures were identified along with two bands at 1615 and 1600 cm^{-1} (associated with tyrosine and phenylalanine side-chain vibrations). The peak positions for the different protein secondary structures were initially set at 1640, 1670, 1661, 1685 and 1699 (as shown in electronic supplementary material, figure S3), allowing the width and intensity of the peak to vary. After achieving a reasonable fit, the peak positions are allowed to vary, keeping other parameters fixed. Finally, all parameters are allowed to vary to get the best fit. The fraction of each secondary structure component was calculated by dividing the area of the peak corresponding to that secondary structure by the total area of five peaks (reflecting protein secondary structures).

2.3. Mechanical properties

2.3.1. Native silk

The mechanical properties (Young's modulus, true stress at break, true ultimate strain and toughness) were tested using a nanotensile tester (Nano Bionix© Universal Testing System; MTS, Eden Prairie, MN) following a well-established protocol [39,72]. Three or four threads were tested for each spider at room humidity (26–43% RH, 21 ± 1°C) by mounting a 12.58 mm silk thread on a cardboard mount and then extending it at a strain rate of 0.015 s^{-1}. Samples were collected and tested through late spring to late autumn because of seasonality of the spiders used in this study. Normal changes of approximately 20% RH occur indoors, driven by outside changes from day to day, since heating, ventilation and air conditioning systems control for any drastic changes. Care was taken to account for the true cross-sectional area by observing the silk strands under an optical microscope to determine if one or two axial fibres were present. The diameter of the fibre was calculated as the average of the value obtained by analysing the scanning electron microscope images (model JEOL-7401) taken at three random positions of one MA thread using Adobe Photoshop CC 2018 (Adobe Systems Inc., San Jose, CA) (v. 2018 19.1.3). A total of two threads per spider were used to obtain a representative cross-sectional area for the silk from that individual because of the limited availability of samples from Madagascar.

The true stress at break (or tensile strength, σ_T) is calculated as $\sigma_T = (F/A)$, where F is the force required to break the fibre and A is the instantaneous cross-sectional area, assuming isometric volume [73,74]. True strain at break, $\varepsilon_T = \ln(l/l_o)$, where

l is the actual length of thread before it breaks and l_o is the original length of the thread, refers to how much the material has stretched normalized to its original length. The Young's modulus (or stiffness) was obtained from the initial slope of the stress–strain curve in which the relationship between stress and strain was almost linear and is calculated as $E = \sigma/\varepsilon$. Toughness or the area under the stress–strain curve is calculated as $U_t = \sigma * \varepsilon$.

2.3.2. Supercontracted silk

Mechanical properties were also tested for the MA silk strands obtained after supercontraction to eliminate some of the effects of reeling speed. The supercontraction was induced by putting the strands mounted on a piece of cardboard in the humidity chamber, where the humidity can be controlled by purging dry or humid air (obtained by passing N_2 directly or through a deionized water column). To enable maximum supercontraction, air with humidity greater than 75% RH was introduced into the chamber during which the silk strands began to contract and shrink. The amount of shrinkage is species specific and depends upon the chemical composition of the silk. After the silk fully shrinks and visibly shows slack, dry air with humidity less than 10% RH is introduced into the chamber for 90 s. Immediately, the tensile tests were performed with the supercontracted silk strands using the nano-tensile tester following a protocol similar to that of native silk. The nano-tensile tester was used to measure the change in length from the original length to the length after supercontraction; using the volume conservation rule [74], the cross-sectional area was recalculated.

There was variation in room humidity during silk collection and measurement of properties because all tests were performed under room humidity conditions, which can change daily. Some of these differences could have had some small effects on the properties of the silk. However, we believe that these changes are small compared with the variation from species to species. Furthermore, more extreme changes in silk properties occur past 70–75% RH when the MA silk supercontracts (e.g. [50]), and our collection and testing for native silk was below this threshold.

2.3.3. Statistical analysis

We used a Wilk's Lambda multivariate analysis of variance (MANOVA) to determine if the secondary structure and the mechanical properties of native and supercontracted MA silk differed between species. Individual ANOVAs and Tukey's honestly significant difference were used post hoc when needed to identify which pairwise comparisons were significant among variables and among species, respectively. Multivariate pairwise correlations were performed between the overall protein secondary structures and the mechanical properties of native and supercontracted silk, estimated by a pairwise method. Because multiple silk replicates per spider were used for testing, mean values per individual spider were used to avoid pseudoreplication. We performed a Levene's test for normality of variance to determine normality of the data. Only three (percentage of shrinkage, modulus after supercontraction and true strain after supercontraction) out of the 13 variables did not follow a normal distribution with an alpha smaller than 0.05. However, since transforming the data did not result in a better distribution, we used the data as they were. All statistics were conducted in JMP v. 14 (SAS Institute Inc., Cary, NC).

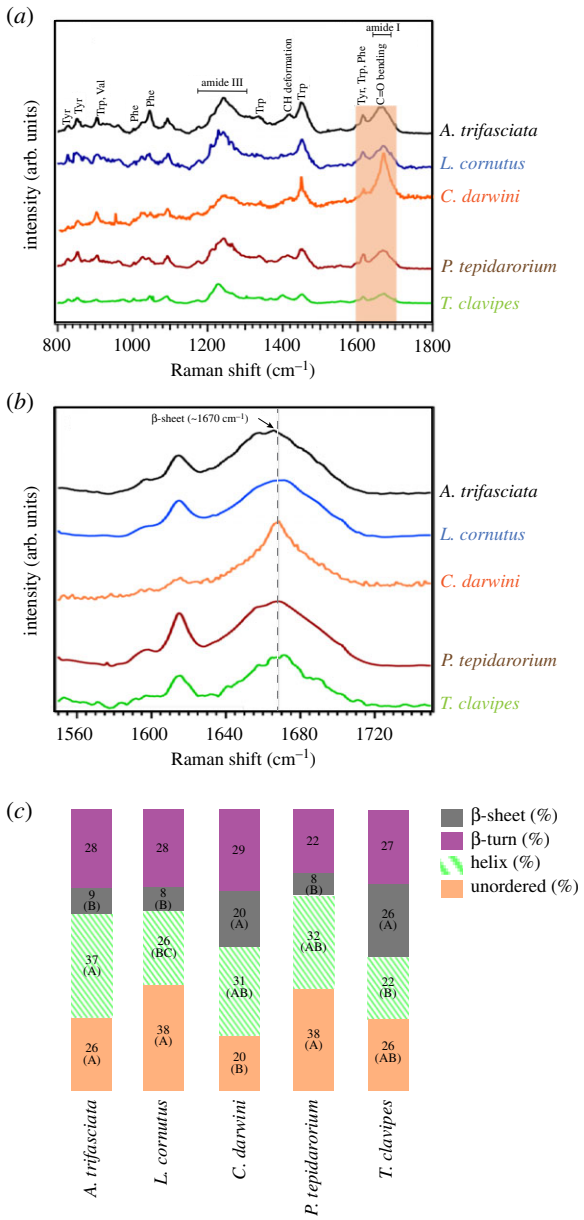

Figure 1. Raman spectra of monofilaments from five species: (*a*) full range (800–1800 cm^{-1}), the shaded region showing the amide I region. (*b*) Enlarged amide I region (1600–1800 cm^{-1}), the dotted line showing the characteristic β-sheet region, approximately 1670 cm^{-1}. (*c*) Calculated percentage of relative protein secondary structures (unordered regions, helices, β-sheets and β-turns) after deconvolution of the amide I region. *C. darwini* silk showed a sharper peak in the amide I region and the highest β-sheet percentage than other species except *T. clavipes*. Only β-sheets (8–26%), unordered regions (20–38%) and helices (22–37%) showed high variation, while β-turns (22–29%) showed no significant variation ($F(4, 11) = 11.66$; $p = 0.001$, $F(4, 11) = 4.82$; $p = 0.017$, $F(4, 11) = 10.89$; $p = 0.001$, $F(4, 11) = 1.09$; $p = 0.408$, respectively). Distinct subgroupings of species for each protein secondary structure identified by post hoc tests are denoted by letters A, B or C (see electronic supplementary material, table S5 for *p*-values), where different letters indicate statistically different percentages.

3. Results

3.1. Composition of protein secondary structures using Raman spectroscopy

Raman spectra of MA silk obtained from four orb web species (*A. trifasciata*, *L. cornutus*, *C. darwini* and *T. clavipes*) and one cobweb species (*P. tepidariorum*) show similar peaks, characteristic of MA silk, in the 800–1800 cm^{-1} range (figure 1*a*). The typical peaks of tyrosine (Y) occur at 830 and 850 cm^{-1} [75], while those of phenylalanine (F) appear at 1004 and 1029 cm^{-1} [59]. However, the ratio of 1413 and 1450 cm^{-1} peaks, representing the C–H deformation

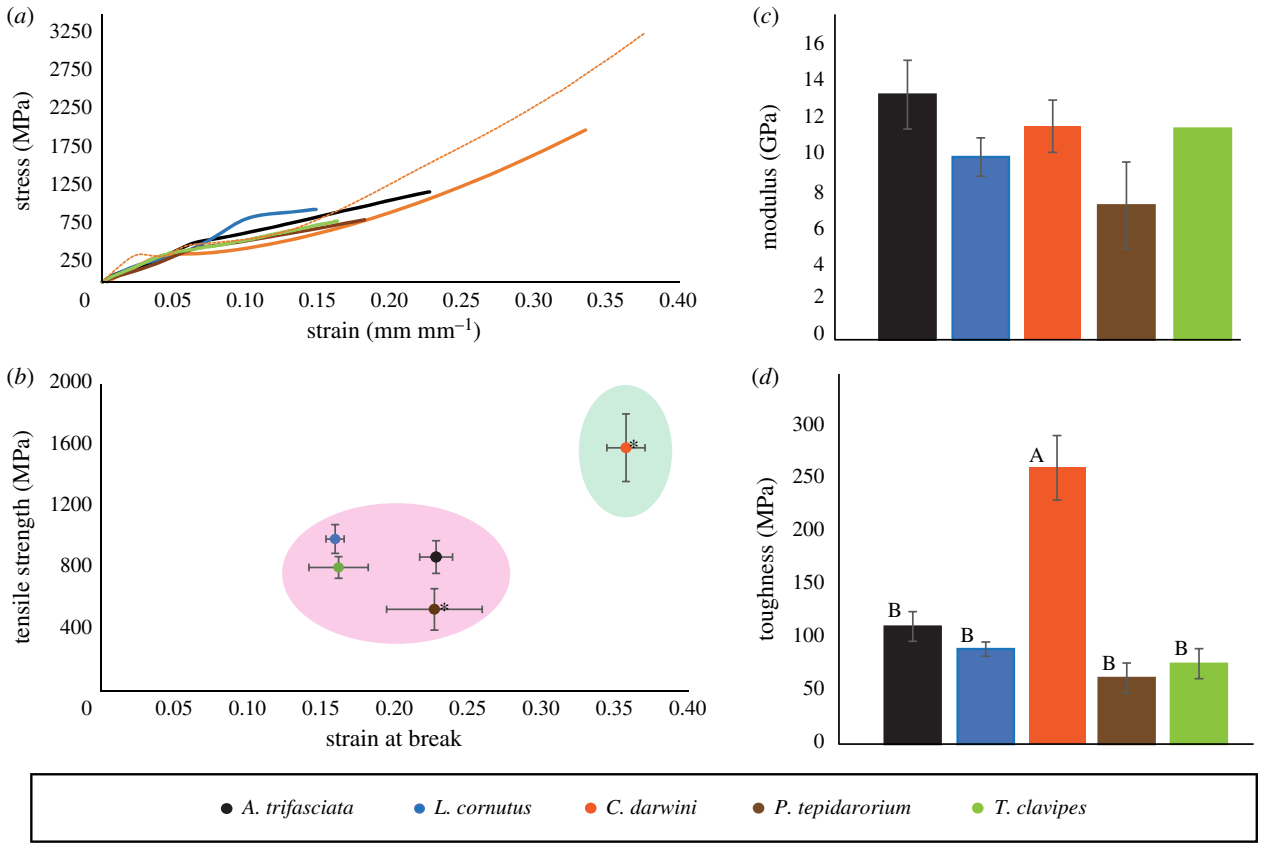

Figure 2. Material properties of native silk from five spider species. (*a*) Representative true stress-true strain curves for all groups. The dotted orange line shows the maximum toughness for the silk of an individual *C. darwini*, while the solid orange line shows a more typical result. (*b*) The average and standard error of the tensile strength and strain at break of all groups. Silk samples enclosed in the same colour circle have statistically indistinguishable strains ($F(4, 23) = 20.39$; $p < 0.001$). The two groups marked by the asterisk have significantly different tensile strength from each other ($F(4, 23) = 4.98$; $p = 0.005$). (*c*) The average and standard error of the modulus ($F(4, 23) = 1.35$; $p = 0.283$). (*d*) The averages and standard error of the toughness for all the groups. The same letter represents the same toughness ($F(4, 23) = 12.14$; $p < 0.001$). See electronic supplementary material, table S5 for post hoc pairwise *p*-values.

near the amide II region (1450–1550 cm^{-1}), appears to be different across species (figure 1*a*). The amide I region (1600–1700 cm^{-1}, plotted in figure 1*b*) provides information about the relative percentage of different protein secondary structures. A visual comparison of the amide I region for all the spider species with respect to *C. darwini* shows that the β-sheet peak (approx. 1670 cm^{-1}) is shifted to the left (by 1–2 cm^{-1}) for *A. trifasciata*, and to the right (by 1–2 cm^{-1}) for *L. cornutus* and *T. clavipes*. We deconvoluted the amide I region to calculate the relative percentage of various protein secondary structures using a protocol established in the literature [15,59,61,63,70,71]. Previous work by Lefèvre *et al.* [70] has shown that it is important to calculate an orientation-insensitive Raman spectrum, especially for anisotropic silk samples, by combining different polarization Raman spectra. However, it was challenging to collect spectra in different polarizations because of instrumental constraints and a large sample set. Thus, the percentages of various protein secondary structures reported in our study may be influenced by the anisotropy of samples, but we do not expect the major differences between the reported values in our study and the ones calculated from orientation-insensitive spectra (more details can be found in electronic supplementary material, figures S1 and S2 and table S1). Overall, the percentages of different secondary structures differ between species ($F(12, 24.10) = 5.40$; $p = 0.001$) (figure 1*c* and electronic supplementary material, table S4). In particular, the percentage of β-sheets in MA silk of *C. darwini* (20 ± 2%) is relatively high compared with other species except *T. clavipes* (26 ± 2%), while the percentage of unordered regions is the least (20 ± 2%) (figure 1*c* and electronic supplementary material, table S4). The percentage of helices in the *C. darwini* silk is relatively high compared with *L. cornutus* and *T. clavipes*, but not significantly different from *A. trifasciata* and *P. tepidadorium*. A comparison across different spider species reveals no significant difference in the percentage of β-turns (22–29%; electronic supplementary material, tables S4 and S5 for ANOVA and post hoc results). However, the percentage of β-sheets is higher among *C. darwini* (20%) and *T. clavipes* (26%) than among the rest of the species studied in the present work (figure 1*c* and electronic supplementary material, table S4). The percentage of helices is the lowest in the silk extracted from *T. clavipes* compared with others except *L. cornutus*. Finally, the percentage of unordered regions for *C. darwini* is lower than that for *L. cornutus* and *P. tepidadorium*.

3.2. Mechanical properties

The four mechanical properties tested for our four species and *C. darwini* MA silk are compared in figure 2. Figure 2*a* shows the representative stress–strain plots for MA silk obtained from five spider species: one cobweb spider (*P. tepidarorium*) and four orb web spiders (*A. trifasciata*, *L. cornutus*, *T. clavipes* and *C. darwini*). Overall, the mechanical properties differ between species ($F(12, 55.85) = 4.865$; $p < 0.001$) (figure 2

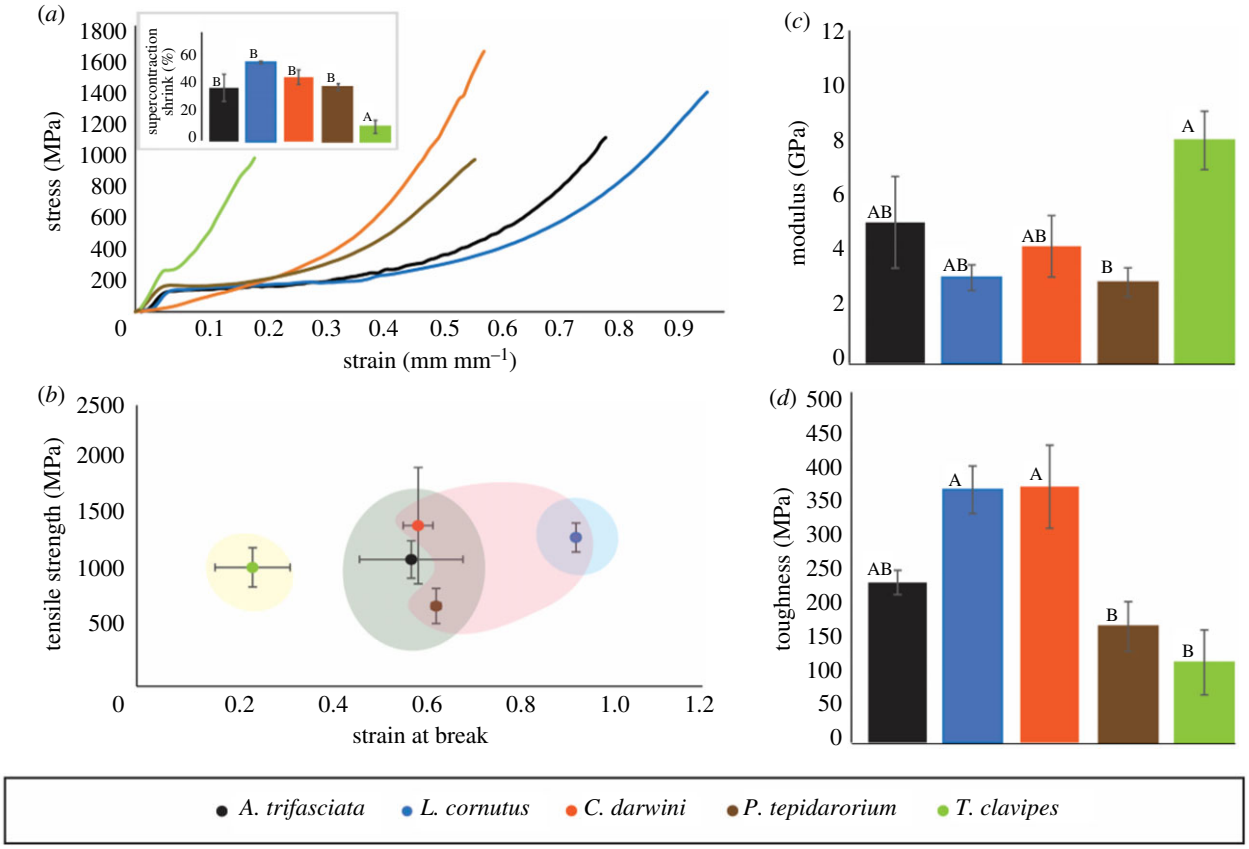

Figure 3. Material properties of maximally supercontracted silk of five spider species. (*a*) Representative true stress-true strain curves for all groups. Inset shows the per cent shrinkage of silk during supercontraction, with the same letter showing the same shrinkage ($F(4, 15) = 7.1768$; $p = 0.0019$). (*b*) The average and standard error of the tensile strength and strain at break of all groups. Silk samples enclosed in the same colour circle have the same strains ($F(4, 15) = 10.90$; $p < 0.001$). The stress is not statistically different ($F(4, 15) = 1.41$; $p = 0.280$). (*c*) The average and standard error of the modulus. Statistically different groups are shown by different letters ($F(4, 15) = 3.19$; $p = 0.0.043$). (*d*) The averages and standard error of the toughness for all the groups. The same letter represents the same toughness ($F(4, 15) = 8.74$; $p < 0.001$). See electronic supplementary material, table S5 for post hoc pairwise *p*-values.

and electronic supplementary material, table S4). One-way ANOVA showed that species varied significantly for three out of four of the measured silk mechanical properties (electronic supplementary material, tables S4 and S5). *C. darwini* silk shows the highest ultimate strength, statistically different from *P. tepidarorium* (figure 2*b*), while ultimate strength does not vary among other species. Strain at break (or extensibility) varies more than twofold from 0.16 ± 0.01 to 0.35 ± 0.02 (figure 2*b*), with dragline silk from *L. cornutus* and *T. clavipes* having the lowest, and *C. darwini* having the highest, strain at break (electronic supplementary material, table S2). The strain at break measured in the present study for *C. darwini* MA silk is lower than the literature-reported strain of 0.9 (figure 2*b*; [6]). Stiffness (or Young's modulus) did not differ between the silks tested (figure 2*c*). The mean toughness of *C. darwini* MA silk (261 ± 31 MPa) is significantly higher than all other tested species (figure 2*d*).

After supercontraction of silk, overall strength, extensibility and toughness increased for all species, while stiffness decreased (except for *T. clavipes*), relative to the properties of each species silk before supercontraction (figure 3). The mechanical properties of silk after supercontraction also differed between species ($F(16, 37.30) = 2.603$; $p = 0.008$) (figure 3 and electronic supplementary material, table S4). *T. clavipes* stiffness remained almost unchanged, which was not surprising as it only shrank 10% of its original length during supercontraction (inset figure 3*a*). However, the interspecies differences in tensile strength disappeared between all species after supercontraction (figure 3*b*). On the other hand, differences in strain at break and toughness (figure 3*b*) persisted. While most groups showed an increase in the extensibility, stretching over 50% of its original length, *L. cornutus* had a strain of almost 100%, surprisingly achieving the same toughness as MA silk of *C. darwini* (*L. cornutus* reaching 375 ± 35 MPa and *C. darwini* 380 ± 62 MPa), as mentioned in electronic supplementary material, table S2. By contrast, all other species had an average toughness below 170 MPa, with the exception of *A. trifasciata*, which had an average toughness of 237 MPa (figure 3*d* and electronic supplementary material, table S4). After supercontraction, interspecies differences in stiffness were also observed, with *P. tepidarorium* showing the lowest stiffness and *T. clavipes* showing the highest stiffness.

3.3. Correlation between mechanical properties and relative protein secondary structure

Since our primary goal is to understand the correlation between the molecular-level relative protein secondary structures and the observed mechanical properties, figure 4*a–l* and electronic supplementary material, table S3 show the regression plots and eye-guide of the various mechanical properties (toughness, modulus, strain at break and tensile strength) against different protein secondary structures (β-sheets, β-turns and unordered regions) before supercontraction for all species. Both toughness ($r = 0.57$, $p = 0.032$)

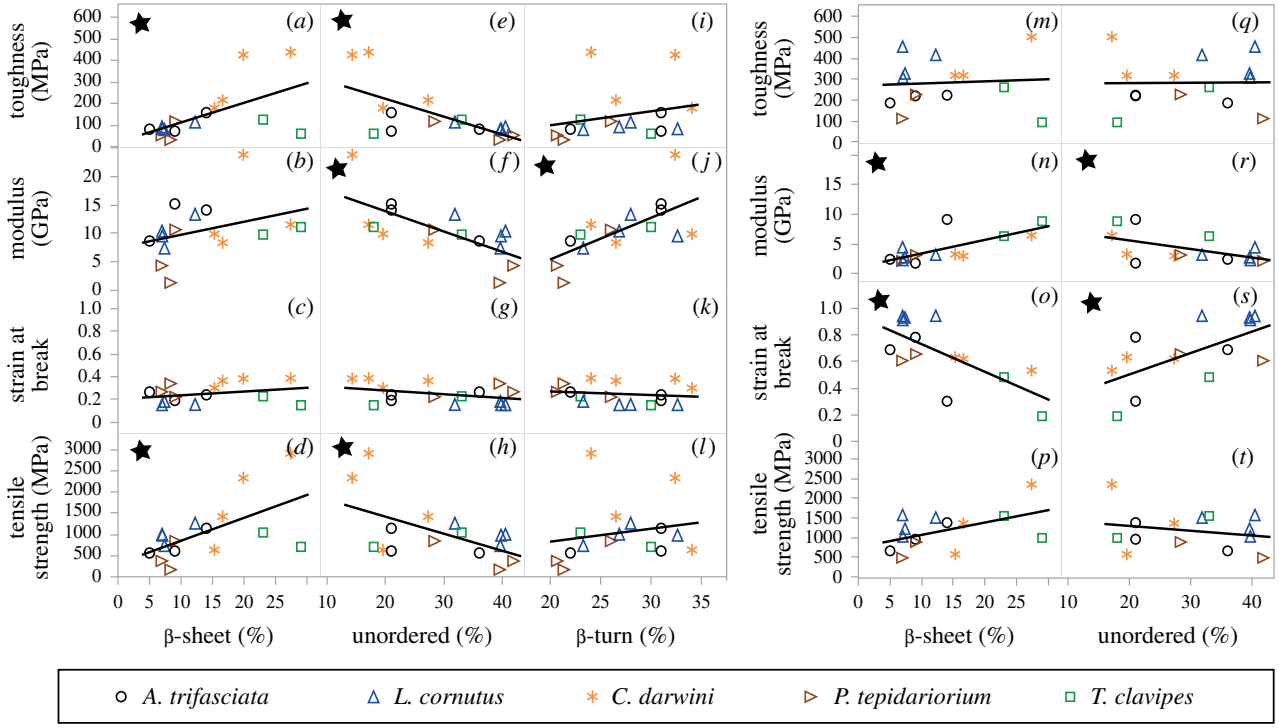

Figure 4. Correlation between relative protein secondary structure and mechanical performance of individual spiders before supercontraction (*a–l*) and after supercontraction (*m–t*). Before supercontraction, β-sheet content shows a positive correlation with both toughness ($r = 0.57$, $p = 0.032$) and tensile strength ($r = 0.59$, $p = 0.026$). Toughness ($r = -0.66$, $p = 0.011$), modulus ($r = -0.70$, $p = 0.005$) and tensile strength ($r = -0.06$, $p = 0.001$) show a negative correlation with the percentage of unordered regions. The percentage of β-turns unexpectedly affects the modulus ($r = 0.06$, $p = 0.001$). After reducing spinning effects by supercontraction, β-sheet content shows a positive correlation with modulus ($r = 0.63$, $p = 0.017$) and a negative correlation with strain at break ($r = -0.71$, $p = 0.005$), while unordered content has the opposite trend: a positive correlation with strain at break ($r = 0.63$, $p = 0.017$) and a negative correlation with modulus ($r = -0.53$, $p = 0.051$). Significant relationships are marked by stars.

and tensile strength ($r = 0.59$ $p = 0.026$) show a positive correlation with the percentage β-sheet content in the MA silk (figure 4*a*,*d*). The positive correlation of tensile strength on β-sheet content as seen in figure 4*d* is consistent with literature measurements with flagelliform and MA silk of *T. clavipes*, *Araneus diadematus* and *Argiope aurantia* [15]. In comparison, the toughness ($r = -0.66$, $p = 0.011$), modulus ($r = -0.70$, $p = 0.005$) and tensile strength ($r = -0.55$, $p = 0.040$) showed a negative correlation with the percentage of unordered regions (figure 4*e–h*). Unexpectedly, the percentage of β-turns has a positive correlation with the modulus ($r = 0.07$, $p = 0.001$), but not strain at break (figure 4*j*,*l*).

We also correlated the measured mechanical properties after supercontraction of silk with the percentage of secondary structures obtained before supercontraction. Previous work by Dionne *et al*. [64] and Dong *et al*. [53] has demonstrated a change of only 3–5% in the percentage of β-sheets and unordered regions after supercontraction of MA silk. Considering the percentage error in the calculated relative protein secondary structures in our study (±2%), we do not expect this small change to perturb the correlation between the mechanical properties and the relative protein secondary structures although it remains to be verified in further studies. After supercontraction (figure 4*m–t* and electronic supplementary material, table S3), the modulus shows a clear positive correlation with the percentage of β-sheets and negative dependence on the percentage of unordered regions ($r = 0.73$, $p = 0.003$ and $r = -0.53$, $p = 0.051$, respectively). On the other hand, the strain at break shows a negative correlation with respect to β-sheet content and a positive correlation with respect to the unordered content after supercontraction ($r = -0.71$, $p = 0.005$ and $r = 0.63$, $p = 0.017$, respectively), while no such correlation is observed before supercontraction.

4. Discussion

In this study, we examined the relative protein secondary structure composition of MA silk from *C. darwini* and four other species to correlate the silk structure with its performance. We had hypothesized that *C. darwini* MA silk would have a higher percentage of β-turns because of the proline-rich MaSp4 protein present in this silk, resulting in higher extensibility. Interestingly, the percentage of β-turns observed in *C. darwini* is not significantly different from other species even though there is a significant variation in the proline content across these species (3–12%). The expression of MaSp1 relative to MaSp2 is difficult to assess directly and is instead inferred by predicted differences in amino acid ratios predicted from the cDNA sequencing of their gene transcripts. Proline content is a particularly good predictor of expression ratios of MaSp1, with its abundant 'stiffening' motifs, to MaSp2, with its abundant 'elastic' motifs [11,22,25,28,68,76]. For *C. darwini* MA silk, we predicted a higher percentage of elastic β-turns as a consequence of the additional proline-rich MaSp4 protein in the silk, which provides higher amounts of proline-rich motifs. However, the lack of significant difference in β-turns among species indicates that variation in proline in the MA silk (MaSp2 plus MaSp4) may not solely determine the percentage of β-turns in the MA silk. Thus, high proline content alone may not explain the high stretchiness of *C. darwini* MA silk, as suggested in another recent study [8]. Hydroxylated proline is also

shown to play an important role in the silk extensibility. For example, a study with *Argiope keyserlingi* demonstrated a positive correlation between hydroxyl proline and MaSp2 expression, highlighting the connection of hydroxyl proline, MaSp expression and silk extensibility [18]. Nonetheless, we note that *C. darwini* MA silk shows a high percentage of all protein secondary structures (β-turns, β-sheets and helices) except the unordered regions. It is possible that the GPGPX motif in MaSp4 could potentially affect other properties rather than β-turns. Furthermore, we cannot ignore the possibility that other species in this study could have additional, undescribed, MaSp proteins, which could aid in β-turn formation in the MA silk.

In general, as the β-sheet content of the MA silk increases the silk becomes stronger (higher in tensile strength) and tougher. While the same pattern is seen for the β-turn content of the MA silk and its stiffness, MA silk becomes less strong and stiff as the unordered content in the silk increases. However, these correlation dependencies could be influenced by the reeling conditions because the spider could exert muscular control while spinning [77], which can then impact the crystal orientation in MA silk fibre, thus affecting its mechanical properties. Hence, it is important to eliminate some of the effect of reeling on silk's mechanical properties by exposing the silk fibres to a high humidity environment to induce supercontraction [40]. After supercontraction, correlation shows that the silk becomes stiffer and less extensible as the β-sheet content in the silk increases, while the silk fibres are stretchier and more ductile owing to the increase in the unordered content. This is expected because the orientation of amorphous chains becomes more disordered, and stiffness decreases as the silk becomes softer owing to uptake of water molecules [50]. In this state, the molecular chains when exposed to high humidity can reach the favourable thermodynamic state as the plasticization by water molecules enhances the chain mobility. As a result, β-sheet content shows a negative correlation with modulus and a positive correlation with the strain at break after supercontraction (as shown in figure 4), consistent with findings reported in the literature [40]. Assuming that the proportions of different protein secondary structures do not change after supercontraction [53,64], other phenomena such as an increase in water content in the amorphous regions and disruption of hydrogen bonding between chains by water molecules, which lead to changes in orientation of the crystals and molecular chains, could likely explain the observed changes in material properties after supercontraction.

By using the deconvolution method of Raman spectroscopy, we discovered that neither proline abundance *per se* nor proline–glycine neighbouring position (GPGPX) of *C. darwini* MA silk results in different β-turn conformations at a level detectable within the scope of this study. Therefore, the presence of additional proline-rich MaSp4 might not favour β-turn folding, or else favours β-turn folding in contrast to some other opposing factor. Additionally, we cannot exclude the possibility of the presence of MaSp4 in other species in this study (*A. trifasciata*, *L. cornutus*, *P. tepidariorum* and *T. clavipes*), although it has not been described in the literature. It is important to note that the inferences drawn here are based on Raman spectroscopy, which provides limited information. Nonetheless, Raman spectroscopy has been used extensively in the past to characterize the protein secondary structures. We understand that additional information, including percentage crystallinity, crystal size and orientation, is necessary to build a complete structure–property relationship, which would be the scope of our future work.

It is important to note that the *C. darwini* silk (before supercontraction) characterized in this study is not as stretchy as the previously reported value of 0.52 average strain (and the maximum value of 0.9 strain at break) [6]. However, the *C. darwini* MA silk still has a higher extensibility value of 0.35, larger than other species. This could probably be the result of the limited sample size in this study. Nevertheless, it appears that the high extensibility of *C. darwini* silk is not explained simply by a higher fraction of β-turns relative to other protein secondary structures. This finding does not support the second hypothesis that MaSp4 enables a high β-turn content in *C. darwini* MA silk that would result in high stretchiness and thereby contribute to its high toughness. However, we cannot exclude the possibility that MaSp4 acts to maintain β-turn content in interaction with some other factor that is normally contrary to extensibility, such as the relatively high β-sheet content of *C. darwini* MA silk. In the future, we need to examine differences in the sizes of the β-sheet nanocrystals and their orientation to build a more comprehensive model. Additional work is needed to explore the role of the longer duct in the MA gland of *C. darwini* and how it influences the silk microstructure.

5. Conclusion

C. darwini MA silk shows exceptional toughness compared with the other spider species used in the present work. The analysis of Raman spectra for MA silk of *C. darwini* and other species highlights differences in the percentage of β-sheets, helices and unordered regions. However, the percentage of β-turns is not different across the different species, suggesting that the presence of extra proline-rich MaSp4 in *C. darwini* MA silk does not result in higher β-turn formation. Thus, the exceptional toughness of MA silk of *C. darwini* cannot be explained solely by the increased percentage of β-turns.

Correlating the measured mechanical properties against the percentage of various relative protein secondary structures, we find that, before supercontraction, toughness and tensile strength have a positive correlation with the percentage of β-sheets and a negative correlation with the percentage of unordered regions. Also, the modulus has a positive correlation with the β-turn percentage and a negative correlation with the percentage of unordered regions. After supercontraction, modulus has a positive correlation with the percentage of β-sheets, while a negative correlation with the percentage of unordered regions is discovered. The opposite trend is observed for the strain at break.

In summary, while some of the mechanical properties are explained by the percentage of secondary structures, others are not, highlighting that the percentage of various relative protein secondary structures alone may be insufficient to completely explain the mechanical properties. Other parameters such as crystal size, crystal orientation and chain orientation are needed to provide a comprehensive explanation for the observed mechanical properties. This would allow us to understand the structure–property relationships of spider MA silk, thereby helping in the design of high-performance biomaterials.

Data accessibility. The raw data of the mechanical properties, protein secondary structure as well as correlation analysis are available online at the zenodo depository [78].

Additional information is provided in the electronic supplementary material [79].

Authors' contributions. K.Z.H., A.M.A.-S., T.A.B. and A.D. designed the study. K.Z.H. performed the Raman measurements and analysed the data. A.M.A.-S. conducted mechanical tests, analysed data and performed statistical analysis. K.Z.H. and A.M.A.-S. wrote the manuscript. M.M. performed the amino acid analysis and wrote that part. T.A.B., A.D. and S.S. helped in data interpretation and writing and editing the manuscript. I.A. M.K. and M.G. collected the *Caerostris darwini* specimens. I.A., J.E.G., M.K., M.G. and R.A.H. provided helpful suggestions in improving the manuscript. All authors discussed the results and commented on the manuscript.

Competing interests. The authors declare no competing interests.

Funding. This research was supported by the National Science Foundation grants to T.A.B. (IOS-1656645), A.D (IOS-1656645), I.A. (IOS-1656460), J.E.G. and R.A.H. (IOS-1656458). Additional financial support came from the Slovenian Research Agency (Z1-8143, J1-9163, P1-0255 and P1-0236).

References

1. Gosline JM, DeMont ME, Denny MW. 1986 The structure and properties of spider silk. *Endeavour* **10**, 37–43. (doi:10.1016/0160-9327(86)90049-9)
2. Kelly SP, Sensenig A, Lorentz KA, Blackledge TA. 2011 Damping capacity is evolutionarily conserved in the radial silk of orb-weaving spiders. *Zoology* **114**, 233–238. (doi:10.1016/j.zool.2011.02.001)
3. Sensenig AT, Lorentz KA, Kelly SP, Blackledge TA. 2012 Spider orb webs rely on radial threads to absorb prey kinetic energy. *J. R. Soc. Interface* **9**, 1880–1891. (doi:10.1098/rsif.2011.0851)
4. Gosline JM, Guerette PA, Ortlepp CS, Savage KN. 1999 The mechanical design of spider silks: from fibroin sequence to mechanical function. *J. Exp. Biol.* **202**, 3295–3303. (doi:10.1242/jeb.202.23.3295)
5. Kuntner M, Agnarsson I. 2010 Web gigantism in Darwin's hark spider, a new species from Madagascar (Araneidae: Caerostris). *J. Arachnol.* **38**, 346–356. (doi:10.1636/B09-113.1)
6. Agnarsson I, Kuntner M, Blackledge TA. 2010 Bioprospecting finds the toughest biological material: extraordinary silk from a giant riverine orb spider. *PLoS ONE* **5**, 1–8. (doi:10.1371/journal.pone.0011234)
7. Gregorič M, Agnarsson I, Blackledge TA, Kuntner M. 2011 Darwin's bark spider: giant prey in giant orb webs (*Caerostris darwini*, Araneae: Araneidae)? *J. Arachnol.* **39**, 287–295. (doi:10.1636/CB10-95.1)
8. Garb JE, Haney RA, Schwager EE, Gregorič M, Kuntner M, Agnarsson I, Blackledge TA. 2019 The transcriptome of Darwin's bark spider silk glands predicts proteins contributing to dragline silk toughness. *Commun. Biol.* **2**, 1–8. (doi:10.1038/s42003-019-0496-1)
9. Dong Z, Lewis RV, Middaugh CR. 1991 Molecular mechanism of spider silk elasticity. *Arch. Biochem. Biophys.* **284**, 53–57. (doi:10.1016/0003-9861(91)90262-H)
10. Eisoldt L, Smith A, Scheibel T. 2011 Decoding the secrets of spider silk. *Mater. Today* **14**, 80–86. (doi:10.1016/S1369-7021(11)70057-8)
11. Marhabaie M, Leeper TC, Blackledge TA. 2014 Protein composition correlates with the mechanical properties of spider (*Argiope trifasciata*) dragline silk. *Biomacromolecules* **15**, 20–29. (doi:10.1021/bm401110b)
12. Ayoub NA, Garb JE, Tinghitella RM, Collin MA, Hayashi CY. 2007 Blueprint for a high-performance biomaterial: full-length spider dragline silk genes. *PLoS ONE* **2**, e514. (doi:10.1371/journal.pone.0000514)
13. Xu M, Lewis RV. 1990 Structure of a protein superfiber: spider dragline silk. *Proc. Natl. Acad. Sci. USA* **87**, 7120–7124. (doi:10.1073/pnas.87.18.7120)
14. Hinman MB, Lewis V. 1992 Isolation of a clone encoding a second dragline silk fibroin. *Biol. Chem.* **267**, 19 320–19 324. (doi:10.1016/S0021-9258(18)41777-2)
15. Lefèvre T, Pézolet M. 2012 Unexpected β-sheets and molecular orientation in flagelliform spider silk as revealed by Raman spectromicroscopy. *Soft Matter* **8**, 6350. (doi:10.1039/c2sm25351h)
16. Sirichaisit J, Brookes VL, Young RJ, Vollrath F. 2007 Analysis of structure/property relationships in silkworm (*Bombyx mori*) and spider dragline (*Nephila edulis*) silks using Raman spectroscopy. *Biomacromolecules* **4**, 2885–2895. (doi:10.1021/bm0256956)
17. Gorres KL, Raines RT. 2010 Prolyl 4-hydroxylase. *Crit. Rev. Biochem. Mol. Biol.* **45**, 106–124. (doi:10.3109/10409231003627991)
18. dos Santos-Pinto JRA, Arcuri HA, Esteves FG, Palma MS, Lubec G. 2018 Spider silk proteome provides insight into the structural characterization of *Nephila clavipes* flagelliform spidroin. *Sci. Rep.* **8**, 14674. (doi:10.1038/s41598-018-33068-9)
19. Craig HC, Blamires SJ, Sani MA, Kasumovic MM, Rawal A, Hook JM. 2019 DNP NMR spectroscopy reveals new structures, residues and interactions in wild spider silks. *Chem. Commun.* **55**, 4687–4690. (doi:10.1039/C9CC01045A)
20. Craig HC, Piorkowski D, Nakagawa S, Kasumovic MM, Blamires SJ. 2020 Meta-analysis reveals materiomic relationships in major ampullate silk across the spider phylogeny. *J. R. Soc. Interface* **17**, 20200471. (doi:10.1098/rsif.2020.0471)
21. Hayashi CY, Lewis RV. 1998 Evidence from flagelliform silk cDNA for the structural basis of elasticity and modular nature of spider silks. *J. Mol. Biol.* **275**, 773–784. (doi:10.1006/jmbi.1997.1478)
22. Blamires SJ, Wu C-LL, Blackledge TA, Tso I-MM. 2012 Post-secretion processing influences spider silk performance. *J. R. Soc. Interface* **9**, 2479–2487. (doi:10.1098/rsif.2012.0277)
23. Blamires SJ, Wu CL, Tso IM. 2012 Variation in protein intake induces variation in spider silk expression. *PLoS ONE* **7**, e31626. (doi:10.1371/journal.pone.0031626)
24. Rauscher S, Baud S, Miao M, Keeley FWW, Pomès R. 2006 Proline and glycine control protein self-organization into elastomeric or amyloid fibrils. *Structure* **14**, 1667–1676. (doi:10.1016/j.str.2006.09.008)
25. Savage KN, Gosline JM. 2008 The effect of proline on the network structure of major ampullate silks as inferred from their mechanical and optical properties. *J. Exp. Biol.* **211**, 1937–1947. (doi:10.1242/jeb.014217)
26. Shi X, Holland GP, Yarger JL. 2015 Molecular dynamics of spider dragline silk fiber investigated by 2H MAS NMR. *Biomacromolecules* **16**, 852–859. (doi:10.1021/bm5017578)
27. Blamires SJ, Blackledge TA, Tso I-MM. 2017 Physicochemical property variation in spider silk: ecology, evolution, and synthetic production. *Annu. Rev. Entomol.* **62**, 443–460. (doi:10.1146/annurev-ento-031616-035615)
28. Blamires SJ, Chao IC, Tso IM. 2010 Prey type, vibrations and handling interactively influence spider silk expression. *J. Exp. Biol.* **213**, 3906–3910. (doi:10.1242/jeb.046730)
29. Tso IM, Wu HC, Hwang IR. 2005 Giant wood spider *Nephila pilipes* alters silk protein in response to prey variation. *J. Exp. Biol.* **208**, 1053–1061. (doi:10.1242/jeb.01437)
30. Blackledge TA, Pérez-Rigueiro J, Plaza GR, Perea B, Navarro A, Guinea GV, Elices M. 2012 Sequential origin in the high performance properties of orb spider dragline silk. *Sci. Rep.* **782**, 1–5. (doi:10.1038/srep00782)
31. Viney C. 1997 Natural silks: archetypal supramolecular assembly of polymer fibres. *Supramol. Sci.* **4**, 75–81. (doi:10.1016/S0968-5677(96)00059-4)
32. Knight DP, Vollrath F. 1999 Liquid crystals and flow elongation in a spider's silk production line. *Proc. R. Soc. Lond. B* **266**, 519–523. (doi:10.1098/rspb.1999.0667)
33. Pérez-Rigueiro J, Elices M, Llorca J, Viney C. 2001 Tensile properties of *Attacus atlas* silk submerged in liquid media. *J. Appl. Polym. Sci.* **82**, 53–62. (doi:10.1002/app.1822)
34. Casem ML, Tran LPP, Moore AMF. 2002 Ultrastructure of the major ampullate gland of the black widow spider, *Latrodectus hesperus*. *Tissue Cell* **34**, 427–436. (doi:10.1016/S0040816602000836)
35. Römer L, Scheibel T. 2008 The elaborate structure of spider silk: structure and function of a natural high performance fiber. *Prion* **2**, 154–161. (doi:10.4161/pri.2.4.7490)
36. Dicko C, Vollrath F, Kenney JM. 2004 Spider silk protein refolding is controlled by changing pH. *Biomacromolecules* **5**, 704–710. (doi:10.1021/bm034307c)
37. Koeppel A, Laity PR, Holland C. 2020 The influence of metal ions on native silk rheology. *Acta Biomater.* **117**, 204–212. (doi:10.1016/j.actbio.2020.09.045)
38. Knight DP, Vollrath F. 2001 Changes in element composition along the spinning duct in a Nephila

spider. *Naturwissenschaften* **88**, 179–182. (doi:10.1007/s001140100220)

39. Vollrath F, Madsen B, Shao Z. 2001 The effect of spinning conditions on the mechanics of a spider's dragline silk. *Proc. R. Soc. Lond. B* **268**, 2339–2346. (doi:10.1098/rspb.2001.1590)
40. Elices M, Plaza GR, Pérez-Rigueiro J, Guinea GV. 2011 The hidden link between supercontraction and mechanical behavior of spider silks. *J. Mech. Behav. Biomed. Mater.* **4**, 658–669. (doi:10.1016/j.jmbbm.2010.09.008)
41. Asakura T, Yao J, Yang M, Zhu Z, Hirose H. 2007 Structure of the spinning apparatus of a wild silkworm *Samia cynthia ricini* and molecular dynamics calculation on the structural change of the silk fibroin. *Polymer (Guildf)* **48**, 2064–2070. (doi:10.1016/j.polymer.2007.01.071)
42. Riekel C, Bränden C, Craig C, Ferrero C, Heidelbach F, Müller M. 1999 Aspects of X-ray diffraction on single spider fibers. *Int. J. Biol. Macromol.* **24**, 179–186. (doi:10.1016/S0141-8130(98)00084-1)
43. Ramachandra YL, Bali G, Padmalatha Rai S. 2001 Effect of temperature and relative humidity on spinning behaviour of silkworm (*Bombyx mori* L.). *Indian J. Exp. Biol.* **39**, 87–89.
44. Madsen B, Shao ZZ, Vollrath F. 1999 Variability in the mechanical properties of spider silks on three levels: interspecific, intraspecific and intraindividual. *Int. J. Biol. Macromol.* **24**, 301–306. (doi:10.1016/S0141-8130(98)00094-4)
45. Perez-Rigueiro J. 2005 The effect of spinning forces on spider silk properties. *J. Exp. Biol.* **208**, 2633–2639. (doi:10.1242/jeb.01701)
46. Yazawa K, Sasaki U. 2021 Forcibly spun dragline silk fibers from web-building spider *Trichonephila clavata* ensure robustness irrespective of spinning speed and humidity. *Int. J. Biol. Macromol.* **168**, 550–557. (doi:10.1016/j.ijbiomac.2020.12.076)
47. Boutry C, Blackledge TA. 2010 Evolution of supercontraction in spider silk: structure-function relationship from tarantulas to orb-weavers. *J. Exp. Biol.* **213**, 3505–3514. (doi:10.1242/jeb.046110)
48. Savage KN, Gosline JM. 2008 The role of proline in the elastic mechanism of hydrated spider silks. *J. Exp. Biol.* **211**, 1948–1957. (doi:10.1242/jeb.014225)
49. Work RW. 1977 Dimensions, birefringences, and force-elongation behavior of major and minor ampullate silk fibers from orb-web-spinning spiders—the effects of wetting on these properties. *Text. Res. J.* **47**, 650–662. (doi:10.1177/004051757704701003)
50. Blackledge TA, Boutry C, Wong S-C, Baji A, Dhinojwala A, Sahni V, Agnarsson I. 2009 How super is supercontraction? Persistent versus cyclic responses to humidity in spider dragline silk. *J. Exp. Biol.* **212**, 1981–1989. (doi:10.1242/jeb.028944)
51. Tokareva O, Jacobsen M, Buehler M, Wong J, Kaplan DL. 2014 Structure-function-property-design interplay in biopolymers: spider silk. *Acta Biomater.* **10**, 1612–1626. (doi:10.1016/j.actbio.2013.08.020)
52. Kuntner M *et al.* 2019 Golden orbweavers ignore biological rules: phylogenomic and comparative analyses unravel a complex evolution of sexual size dimorphism. *Syst. Biol.* **68**, 555–572. (doi:10.1093/sysbio/syy082)
53. Dong Q, Fang G, Hu L, Yao J, Shao Z, Chen X, Huang Y, Ling S. 2019 Effect of stress on the molecular structure and mechanical properties of supercontracted spider dragline silks. *J. Biomed. Mater. Res. B Appl. Biomater.* **8**, 168–176. (doi:10.1039/c9tb02032b)
54. Kong N *et al.* 2020 A cuboid spider silk: structure–function relationship and polypeptide signature. *Macromol. Rapid Commun.* **1900583**, 1–7. (doi:10.1002/marc.201900583)
55. Fu C, Porter D, Chen X, Vollrath F, Shao Z. 2011 Understanding the mechanical properties of *Antheraea pernyi* silk—from primary structure to condensed structure of the protein. *Adv. Funct. Mater.* **21**, 729–737. (doi:10.1002/adfm.201001046)
56. Jenkins JE, Creager MS, Butler EB, Lewis RV, Yarger JL, Holland GP. 2010 Solid-state NMR evidence for elastin-like β-turn structure in spider dragline silk. *Chem. Commun.* **46**, 6714–6716. (doi:10.1039/c0cc00829j)
57. Jenkins JE *et al.* 2013 Characterizing the secondary protein structure of black widow dragline silk using solid-state NMR and X-ray diffraction. *Biomacromolecules* **14**, 3472–3483. (doi:10.1021/bm400791u)
58. McGill M, Holland GP, Kaplan DL. 2019 Experimental methods for characterizing the secondary structure and thermal properties of silk proteins. *Macromol. Rapid Commun.* **40**, 1800390. (doi:10.1002/marc.201800390)
59. Lefèvre T, Paquet-Mercier F, Rioux-Dubé JF, Pézolet M. 2012 Review: structure of silk by Raman spectromicroscopy: from the spinning glands to the fibers. *Biopolymers* **97**, 322–336. (doi:10.1002/bip.21712)
60. Rousseau M-E, Lefèvre T, Beaulieu L, Asakura T, Pézolet M. 2004 Study of protein conformation and orientation in silkworm and spider silk fibers using Raman microspectroscopy. *Biomacromolecules* **5**, 2247–2257. (doi:10.1021/bm049717v)
61. Lefèvre T, Rousseau ME, Pézolet M. 2007 Protein secondary structure and orientation in silk as revealed by Raman spectromicroscopy. *Biophys. J.* **92**, 2885–2895. (doi:10.1529/biophysj.106.100339)
62. Rousseau ME, Lefèvre T, Pézolet M. 2009 Conformation and orientation of proteins in various types of silk fibers produced by *Nephila clavipes* spiders. *Biomacromolecules* **10**, 2945–2953. (doi:10.1021/bm9007919)
63. Dionne J, Lefèvre T, Auger M. 2016 Major ampullate spider silk with indistinguishable spidroin dope conformations leads to different fiber molecular structures. *Int. J. Mol. Sci.* **17**, 1353. (doi:10.3390/ijms17081353)
64. Dionne J, Lefèvre T, Bilodeau P, Lamarre M, Auger M. 2017 A quantitative analysis of the supercontraction-induced molecular disorientation of major ampullate spider silk. *Phys. Chem. Chem. Phys.* **19**, 31 487–31 498. (doi:10.1039/c7cp05739c)
65. Guinea GV, Elices M, Pérez-Rigueiro J, Plaza GR. 2004 Stretching of supercontracted fibers: a link between spinning and the variability of spider silk. *J. Exp. Biol.* **208**, 25–30. (doi:10.1242/jeb.01344)
66. Fu C, Porter D, Shao Z. 2009 Moisture effects on *Antheraea pernyi* silk's mechanical property. *Macromolecules* **42**, 7877–7880. (doi:10.1021/ma901321k)
67. Garb JE, Ayoub NA, Hayashi CY. 2010 Untangling spider silk evolution with spidroin terminal domains. *BMC Evol. Biol.* **10**, 1–16. (doi:10.1186/1471-2148-10-243)
68. Liu Y, Sponner A, Porter D, Vollrath F. 2008 Proline and processing of spider silks. *Biomacromolecules* **9**, 116–121. (doi:10.1021/bm700877g)
69. Hayashi CY, Shipley NH, Lewis RV. 1999 Hypotheses that correlate the sequence, structure, and mechanical properties of spider silk proteins. *Int. J. Biol. Macromol.* **24**, 271–275. (doi:10.1016/S0141-8130(98)00089-0)
70. Lefèvre T, Rousseau M-EE, Pézolet M. 2006 Orientation-insensitive spectra for Raman microspectroscopy. *Appl. Spectrosc.* **60**, 841–846. (doi:10.1366/000370206778062039)
71. Rousseau M-E, Beaulieu L, Lefèvre T, Paradis J, Asakura T, Pézolet M. 2006 Characterization by Raman microspectroscopy of the strain-induced conformational transition in fibroin fibers from the silkworm *Samia cynthia ricini*. *Biomacromolecules* **7**, 2512–2521. (doi:10.1021/bm060280w)
72. Sensenig A, Agnarsson I, Blackledge TA. 2010 Behavioural and biomaterial coevolution in spider orb webs. *J. Evol. Biol.* **23**, 1839–1856. (doi:10.1111/j.1420-9101.2010.02048.x)
73. Vollrath F, Madsen B, Shao Z, Vollrath F, Vladsent B, Shao Z. 2001 The effect of spinning conditions on the mechanics of a spider's dragline silk. *Proc. R. Soc. Lond. B* **268**, 2339–2346. (doi:10.1098/rspb.2001.1590)
74. Guinea GV, Pérez-Rigueiro J, Plaza GR, Elices M. 2006 Volume constancy during stretching of spider silk. *Biomacromolecules* **7**, 2173–2177. (doi:10.1021/bm060138v)
75. Shao Z, Vollrath F, Sirichaisit J, Young RJ. 1999 Analysis of silk in native and supercontracted states using Raman spectroscopy. *Polymer (Guildf)* **40**, 2493–2500. (doi:10.1016/S0032-3861(98)00475-3)
76. Tso IM, Chiang SY, Blackledge TA. 2007 Does the giant wood spider *Nephila pilipes* respond to prey variation by altering web or silk properties? *Ethology* **113**, 324–333. (doi:10.1111/j.1439-0310.2007.01318.x)
77. Gosline J. 2018 *Mechanical design of structural materials in animals*, p. 179. Princeton, NJ: Princeton University Press.
78. Zin Htut K *et al.* 2021 Data from: Correlation between protein secondary structure and mechanical performance for the ultra-tough dragline silk of Darwin's bark spider. Zenodo. (http://doi.org/10.5281/zenodo.4776679)
79. Zin Htut K *et al.* 2021 Data from: Correlation between protein secondary structure and mechanical performance for the ultra-tough dragline silk of Darwin's bark spider. Collection. (https://doi.org/10.6084/m9.figshare.c.5448661)